

# **Thermospheric dark band structures observed in all-sky OI 630 nm emission images over the Brazilian low-latitude sector**

A. A. Pimenta<sup>1</sup>, M.C. Kelley<sup>2</sup>, Y. Sahai<sup>1,3</sup>, J.A. Bittencourt<sup>1</sup> and P.R. Fagundes<sup>3</sup>

<sup>1</sup> Instituto Nacional de Pesquisas Espaciais (INPE), Sao Jose dos Campos, SP, Brazil

<sup>2</sup> School of Electrical Engineering, Cornell University, Ithaca, New York. U.S.A.

<sup>3</sup> Universidade do Vale do Paraíba (Univap), Sao Jose dos Campos, SP, Brazil

## **Abstract**

Using two ground-based all-sky imaging systems, measurements of moving dark band structures in the OI 630.0 nm nightglow emission were detected in the low-latitude region of Brazil. On the nights of August 30-31, 1995, July 18-19, 1998 and July 13-14, 1999, the all-sky imaging observations of the OI 630 nm emission, carried out at Cachoeira Paulista (22.7°S, 45°W, magnetic declination 20°W), Brazil, showed dark band structures which stretched across the entire image and which propagated from southeast to northwest. The observed band structures are thus most likely formed in the mid-latitude region and move into the field of view. Digisonde observations, available for two of the events, registered abrupt increases in both the F-layer peak height ( $h_mF_2$ ) and minimum virtual height ( $h'F$ ) on July 19, 1998 and July 13, 1999, when the low intensity band passed over Cachoeira Paulista. It should be pointed out that these thermospheric events are not related to geomagnetic disturbed conditions, as the nights for which data are presented are geomagnetically quiet ( $K_p < 2$ ). In this paper, we present and discuss the first observations of these thermospheric dark band structures in the Brazilian sector and their effects on the nighttime ionosphere. A possible mechanism for generation of these dark band structures is presented.

## 1 - Introduction

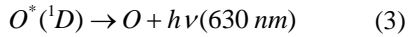
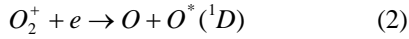
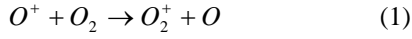
The physics of the relationship between atmospheric gravity waves (AGW) and traveling ionospheric disturbances (TIDs) has been studied by a large number of authors throughout the last four decades since the pioneering paper by Hines (1960) who postulated that the TIDs frequently seen in ionosphere data are mainly caused by AGWs in the thermosphere. A classification of ionosphere/thermosphere waves according to their periods is common and can be done as follows: travelling ionospheric disturbances with periods from some minutes to several hours, gravity waves with periods from about 10 minutes to few hours, tides as a global wave with harmonics of a 24h period and planetary waves with still longer periods. The first two categories overlap in period and it is clear that they are related.

TIDs have been observed by various techniques since the 1950's (see Hunsucker [1982] for a review). The discrimination of TIDs into large-scale TIDs (LSTIDs) and medium-scale TIDs (MSTIDs) is related to their horizontal wavelength,  $\lambda$ , and roughly speaking the former correspond to  $\lambda > 1000$  km and the latter to  $\lambda < 1000$  km. Less concrete is a parsing based on their periods, with LSTIDs associated with periods from about 30-60 min to several hours, while MSTIDs are described as having periods from about 10 to 40-60 min. Large-scale traveling ionospheric disturbances are characteristic of the storm-time mid-latitude ionosphere. They have a horizontal scale of more than 1000 km and propagate equatorward with a velocity in the range 400-1000 m/s [Hunsucker, 1982]. These disturbances are almost certainly caused by thermospheric neutral waves generated by the auroral zone energy input. As they push plasma up and down the magnetic field lines at mid-latitudes the TID is generated in a fairly straightforward manner. A recent spectacular event of this type was documented over Arecibo and North America by Nicolls et al. (2004).

Optical measurements of MSTIDs which we refer to here as Dark Band Structures (DBS) are comparatively rare and only recently have their spatial signatures in the mid-latitude OI 630 nm airglow been reported [Mendillo et al., 1997; Garcia et al., 2000; Kelley et al., 2002, Shiokawa et al., 2005]. Also, in Brazilian low latitude sector, Sobral et al., 1997, reported photometric southern hemisphere wintertime perturbations of the nocturnal F-region OI 630 nm. The events were characterized by south-to-north traveling airglow valleys, or depletions events, with velocities, wavelengths and periods varying within the ranges of 150-300 m/s, 100-200 km and 15 min – 3h, respectively, during quiet and storm periods. Our observations of the MSTID/DBS are not related to geomagnetic disturbed conditions. It is important to note that, unlike equatorial spread F, these structures are not aligned with the magnetic meridian but rather are aligned from NW to SE in the northern hemisphere (Garcia et al, 2000) and SW to NE in the south. Even more importantly, these structures appear simultaneously at the conjugate location which is definitive evidence that they are electrified (Shiokawa et al. 2005). In this paper, using all-sky images in the OI 630 nm emission, we present MSTID events in the Brazilian sector and their effects of the ionization on its propagation in the nighttime thermosphere-ionosphere.

## 2 - Measurement technique and observations

In low-latitude region, the dissociative recombination of  $O_2^+$  in the F-region is the dominant process for producing the excited oxygen atoms that give rise to the OI 630 nm nightglow. The major chemical reactions that generate the OI 630 nm airglow emission in the F-region are as follows:



It is considered that production of  $O(^1D)$  by dissociative recombination of  $NO^+$  is unimportant (Dalgarno and Walker, 1964). Therefore, the production of the OI 630 nm emission depends on the molecular oxygen density  $[O_2]$  and on the oxygen ion density  $[O^+]$ . The oxygen ion density  $[O^+]$  is approximately equal to the electron density in the F-region. The height of the F-layer peak electron density is around 350-400 km, while the molecular oxygen density  $[O_2]$  increases with decreasing height. Thus, the OI 630 nm emission peak occurs in the bottomside of the F-region around 220-300 km. When the F-layer moves upward, the OI 630 nm emission decreases while the plasma density remains unchanged due to the decrease of recombination with height, so that the dark bands in the OI 630 nm emission intensity are a sensitive indicator of F-region vertical motion. When the F layer moves downward the emission increases and the plasma density decreases which tend to cancel out so that the region between the dark bands is more complex and less easy to detect.

With regard to the imaging system, the OI 630 nm emission images presented for August 30-31, 1995 and July 19, 1998 (see Figs 1,3 and 7), were obtained by an all-sky imaging system donated by the Boston University. It uses a 10 cm diameter interference filter with a bandwidth of 1.35 nm and records intensified monochromatic images on 35 mm film using a conventional single lens reflex camera. The images were recorded at interval of 20 min with 40 s exposure time (for more details see Mendillo and Baumgardner, 1982). An important characteristic of the imager is the relationship between zenith angle and image size. A zenith angle of approximately  $90^\circ$  encompasses  $\pm 15^\circ$  latitude/longitude from the zenith, which is equivalent to a horizontal diameter of approximately 3600 km at 275 km altitude. Figure 1 shows the field of view of this system together with other relevant information.

In October 1998 a new all-sky imaging system with CCD camera was put in operation at Cachoeira Paulista, in collaboration with the Utah State University (see Fig. 5). This new all-sky imager has a CCD detector and the images obtained from it have higher resolution when compared with the previous imager. The CCD imager consists of a large area ( $6.45 \text{ cm}^2$ ), high resolution,  $1024 \times 1024$  back-illuminated array with a pixel depth of 14 bits. The images were binned on-chip down to  $512 \times 512$  resolution to enhance the signal-to-noise ratio and were recorded at intervals of 7 minutes with 90 seconds exposure rate.

For each imager the image appears curved and compressed at low elevation angles. Figure 2B shows an example of unwarping all-sky images of Figure 2A using the method described by Garcia et al. (1997). In this figure, an area of the processed image, corresponding to  $360,000 \text{ km}^2$  ( $600 \text{ km} \times 600 \text{ km}$ ) at the airglow layer, is mapped assuming an emission altitude of 275 km. The final geographic coordinate system is a 2-D uniformly spaced grid at the height of the airglow layer.

The spaced imaging measurements provided an opportunity to estimate the physical extent and time history of the DBS. It is possible to determine the DBS parameters such as phase velocity, horizontal wavelength and, consequently, the period in an earth-fixed frame over a wide range of zenith angles. We can determine the horizontal wave parameters directly using standard 2-D FFT analysis. We can investigate DBS content in any part of the image by isolating the region of interest, taking the 2-D FFT of the selected region, and investigating peaks in the squared magnitude of the frequency spectrum. Figure 2B shows an example of this technique where one region was selected, and indicated by the white rectangle that contains a DBS. Figure 2C shows the computed squared magnitude of the 2-D FFT of Figure 2B inside the white rectangle. Owing to the symmetry of the FFT of real data, two mirror-image peaks in the power spectrum are evident at ( $\mathbf{k}_x = \pm 0.06135 \text{ rad/km}$ ,  $\mathbf{k}_y = \mp 0.01840 \text{ rad/km}$ ), corresponding to the quasi-monochromatic wave structure present in 2A. We can determine the horizontal wavelength of this wave by computing the inverse of the distance of the peak from the origin, and it was found to be 100 km. The direction of propagation of the DBS is given (with a  $180^\circ$  ambiguity, again owing to the symmetry of FFT) by the position of the peak in k-space diagram (in this case the wave motion was progressing on a heading of either  $-68^\circ$  or  $112^\circ$ ). This ambiguity can be resolved by using a time sequence of images.

Two methods are available to determine the phase velocity of the wave structures present in the all-sky images (Garcia et al., 1997). In the first method we use a sequence of images after the final geographic coordinate system in the 2-D uniformly spaced grid (unwarped images) to established and scan the optical images to obtain a cross-section of the darkness pattern for each dark band structure. Then, these cross-sectional scans are subjected to a correlation analysis leading to the best fit spatial shifts required to match the time between images. A succession of such space and time shifts leads to a phase velocity versus local time relation for the DBS. The uncertainty in the phase velocity is estimated to be of the order of 10% based on geometrical considerations (variation in the height of the airglow layer) and instrumental resolution (Pimenta et al. 2001). The second method is described on page 6 (first paragraph).

Figure 3 shows a sequence of all-sky images in the OI 630 nm obtained at Cachoeira Paulista from 26:00 LT to 27:20 LT on July 19, 1998, that exhibit a DBS at 26:40 LT. At 26:00 LT, the all-sky image (Figure 3A) also shows dark regions (indicated by arrows) that appear to be a wave structure but which are not as pronounced as at the later time. It appears that the DBS at 26:00 LT was resolved as a series of clear wave crests at 26:40 LT, with a horizontal

wavelength of  $\lambda_i \cong 100 \text{ km}$  (MSTIDs) which later were totally dissipated, as indicated by the image at 27:20 LT (Figure 3C).

A Digisonde 256 (DGS256) located at the same site as the all-sky imager was used to obtain vertical sounding data of the ionosphere. The digisonde can be operated in a number of modes, and during the events reported here was at vertical incidence. The vertical ionograms were automatically scaled by using the ARTIST inversion algorithm (Gamache et al., 1992) to obtain the true height profile and subsequently were checked manually and rescaled where necessary to remove obvious errors. The ARTIST program does not provide an error estimate for  $h_m F_2$ , so an error estimate has been arrived at in the following way. Determining true height profiles by inversion of ionogram traces is a complicated procedure in which many factors, such as underlying ionization and E-F valley, must be taken into account. As a consequence, the determination of a general procedure of error determination is beyond the scope of this work. Nevertheless, we can put limits on the errors in  $h_m F_2$ . Such errors arise primarily from experimental measurement errors in virtual height (minimum virtual height) and  $f_o F_2$  (peak F-region frequency) and from the assumptions made concerning the base height of the ionosphere and E-F valley.

Titheridge (1975) stated that neglecting the underlying ionization at night gives true height errors typically too high by 15 to 60 km at 2 MHz, and 5 to 20 km at 6 MHz. Hence when  $f_o F_2$  is close to 2 MHz, the accuracy of  $h_m F_2$  will depend critically on the model used for underlying ionization. For nighttime ionograms containing no normal E region echoes, ARTIST adopts a standard procedure of using a model E region. Hence the accuracy of the true height profile is very dependent on the model, though again the effects in errors will decrease with height, so that  $h_m F_2$  will be the least affected point on the profile. Experimental errors will arise from random errors in the virtual heights and errors in the layer critical frequencies,  $f_o E$ ,  $f_o F_1$ , and  $f_o F_2$ . Titheridge (1975) considered the effects of random errors of 10 km in virtual height and found that the effect on heights near  $h_m F_2$  was less than 1 km. Of course,  $h_m F_2$ , being the peak height of a layer, is a special case, directly affected by any error in  $f_o F_2$ . The likely error has been estimated by taking a sample of ionograms and varying  $f_o F_2$  by 0.1 MHz, which corresponds to the frequency resolution of the ionograms. In summary, the random measurement error in  $h_m F_2$  is conservatively estimated at  $\pm 15\text{-}20 \text{ km}$  [Titheridge (1975)].

The digisonde observations (Figure 4B), around 27:20 LT, registered abrupt increases in  $f_o F_2$  (peak electron density), whereas both the base height ( $h'F$ ) and F-layer peak height ( $h_m F_2$ ) decreased to an altitude of 220 km and 300 km (Figure 4A), respectively, which is the typical altitude range of the OI 630 nm airglow emission. Both of these effects (larger  $f_o F_2$  and lower  $h_m F_2$ ) enhance the airglow. We believe that the bright region which reached the zenith in Figure 3C can be related with the so-called “brightness wave” (BW) reported by Colerico et al. (1996) and Colerico et al. (2002). Colerico et al. (1996), using optical and radio measurements techniques (all-sky CCD airglow imaging system, Fabry-Perot interferometer and ionosonde), showed that during the passage of a BW, the thermospheric

temperatures increase and the meridional wind reverses from equatorward to poleward. Also, the ionosonde recorded decreases in the height of the F-layer during BW events. This supports the concept that the poleward winds generated by the midnight temperature maximum (MTM) pressure bulge cause the lowering of the F-layer to regions of enhanced loss ( $h < 300$  km) and corresponding airglow production. This behavior reported by Colerico et al., 1996, and Colerico et al., 2002, is similar to the event shown in Figures 3B, 3C and 4A of the present study. However, the focus of this study is the dark band structures observed through all-sky the OI 630 nm emission images. It is likely that the BW initially made the DBS more visible in 3B and then may have obscured them as the BW reached zenith.

Figure 5 shows another sequence of the all-sky images in the OI 630 nm emission obtained on July 13, 1999, from 21:47 to 23:55 LT. In this example, a large wave front entered from the southeast and moved across the field of view toward northwest with an average phase velocity of about  $210 \text{ m/s} \pm 10 \text{ m/s}$  (obtained by the image sequence) and passed over Cachoeira Paulista at 23:55 LT. Due to the large wave front, it was not possible to measure the horizontal wavelength using the all-sky images. However, digisonde observations (see Figure 6) registered abrupt increases in both the F-layer peak height ( $h_m F_2$ ) and base height ( $h'F$ ) around 23:30 LT, when the low intensity band passed over Cachoeira Paulista (that coincides with the all-sky image wave front passing over Cachoeira Paulista). This behavior is clearly related to DBS events, which push the F-layer plasma to higher altitudes along the geomagnetic field lines, thus causing the OI 630 nm airglow intensity reduction. Looking at Figure 6C, a defined structure of a 4.5–5.0 hours period with a maximum around 21:00 LT to 29:00 LT can be observed. Also, a weaker peak appears around 19:40 LT, 23:30 LT and 29:00 LT. Considering the large wave front with phase velocity of  $210 \text{ m/s}$  (obtained through the all-sky images sequence) and the period of about 4.5 hours (by the digisonde measurements), we estimated the DBS horizontal wavelength to be about  $\lambda_h \cong 3400 \text{ km}$ . This is quite large for an MSTID but the lack of magnetic activity and the direction seem to rule out a classic LSTID. The event has a sharp edge in the emission strength, which has characteristics of a thermospheric bore wave (which has never been documented) but as argued in the next paragraph, the lack of other characteristics seems to rule this out. Garcia (personal communication, 2002) identified a mesospheric bore in a broadband OH emission, one line of which leaked into the 630 images giving an appearance much like this event.

On August 30-31, 1995 (Figure 7), we have a spectacular event of a DBS in the all-sky images. It is possible to see a passage, through the OI 630 nm emission of a dark front across the entire field of view propagating from southeast to northwest with average speed of about  $250 \text{ m/s}$  at an altitude of 220-300 km. By 25 LT the next phase of enhanced brightness was detected. We used the sequence of images to determine the direction of the propagation, indicating in this case a wave front progression towards northwest ( $-70^\circ$ ). As shown by the arrow in Figure 7, the DBS becomes most active at pre-midnight local time and tends to cease after midnight. Unfortunately, we do not have digisonde

observation for this night from Cachoeira Paulista. In addition, this thermospheric event has one characteristic (presence of an extended dark or bright front) similar to the mesospheric bore detected for the first time by Taylor et al., (1995). However, according to Dewan and Picard (1998), the identification criteria for mesospheric bore are as follows: (1) presence of an extended dark (or bright) front; (2) dark (or bright) front followed by some wave trains; (3) simultaneous occurrence of the front in the different airglow layers without phase lag; (4) presence of wave ducting conditions, thermal and/or Doppler. The event in Figure 7 exhibits only the first criterion according to the bore definition and could not be characterized as a thermospheric bore. If we estimate the wavelength using the adjacent bright bands at 25 LT we obtain about 1000 km for a horizontal wavelength and period of about 4000 s, a little more than an hour.

### 3 – Discussion

The conjugacy of MSTIDs is clear evidence for their electrified nature as is the direct measurement of associated electric fields on spacecraft (Saito et al, 1995) and with incoherent scatter radar (Behnke, 1979; Kelley et al., 2000). This has even led to the suggestion of the term electrobuoyancy wave by Kelley and Miller (1997) to describe them. In the next paragraphs we explore the interaction of the neutral and ionized gases. This is followed by a review of the Perkins' Instability (Perkins, 1973) as a source of MSTIDs.

***Coupling of neutral and ionized gases in the ionosphere.*** If we consider a DBS to be primarily a neutral wave phenomenon then its interaction with the ionization in the F-region via ion-neutral collisions can be discussed by the magnetohydrodynamic absorption theory. Since the ionospheric F-region is a weakly ionized gas, we assume that the propagation of the wave is supported solely by the neutral component of the atmosphere, but that the ionized portion of the atmosphere is set into motion by neutral-ion collisions. Under this hypothesis the ionization effects on the propagation of the DBS events can be deduced from the brightness pattern seen in Figure 3 from 26:00 LT to 27:20 LT and in Figure 4B around 27:00 LT. A good parameter to explain the magnetohydrodynamic absorption of these moving disturbances, in the F-region, is the magnitude of the index of absorption. According Gershman and Grigor'yev (1965) this index can be written as

$$R = G \left[ 1 + k_x^2 / k_z^2 - (\cos \alpha - \cos \gamma / k_z)^2 \right] \quad (1)$$

where  $G = N_e M v_{im} k_x / N_m M_m \omega$ , and  $\cos \alpha$ ,  $\cos \beta$  and  $\cos \gamma$  are the projections, on the  $x$ ,  $y$  and  $z$  axis, respectively, of the magnetic field direction on a Cartesian coordinate system ( $x$  is positive to northward,  $y$  to eastward and  $z$  to upward).  $N_e$  is the electron density,  $M$  is the ion mass,  $v_{im}$  is the ion-molecule collision frequency,  $\omega$  is the wave angular frequency,  $k_x$  and  $k_z$  are the horizontal and vertical wavenumbers,  $M_m$  is the molecular mass and  $N_m$  is the molecule concentration. In words,  $G$  is the ratio of the neutral ion collision frequency ( $v_{im}$ ) to the wave frequency times the horizontal wavelength (divided by  $2\pi$ ). It is also equal to the ratio of the Joule dissipation per wave period divided by the energy density of the wave times  $(\lambda/2\pi)$ . We can estimate in (1) the value of the factor  $G$  that is independent of the orientation of the magnetic field  $\mathbf{B}$ . Table 1 gives the  $G$  values (in  $\text{cm}^{-1}$ ) for altitudes of 220 km, 250 km and 300 km. In these estimates, we use the phase velocity in the horizontal direction,  $V_{ph} = \omega / k_x = 250 \text{ m/s}$ , obtained by the observations, and the collision frequencies,  $v_{im}$ , for the specified altitudes and data on the electron concentration for nighttime ionosphere. In addition, the molecular concentration was obtained from the MSIS-E-90 model.

On the other hand, the factor in square brackets in Eq. (1) depends on the orientation of the direction of propagation relative to the field  $\mathbf{B}$ . We can compare the  $R$  values for propagation of DBS along the meridian, defined below in Eq. (2) as  $R_m$ , and in the zonal direction, defined in Eq. (3) as  $R_z$ . If we assume that the direction of

propagation in the horizontal plane is parallel to the  $x$ -axis, the direction of the magnetic meridian coincides approximately with the  $x$ -axis and  $\cos\beta = 0$ . Then, from (1) we have

$$R_m = G(\sin\alpha + k_x \cos\alpha / k_z)^2 \quad (2)$$

and for propagation in the east-west direction,  $\cos\alpha = 0$  and we obtain

$$R_z = G(1 + k_x^2 \sin^2\gamma / k_z^2) \quad (3)$$

Titheridge (1973) showed that the disturbances, under the condition  $\omega^2 / k_x^2 C_0^2 \ll 1$ , have  $k_x \ll k_z$ . Then, for very small  $\alpha$  (for example in the equatorial region),  $R_m = G(k_x^2/k_z^2)$ , and  $R_z = G$ . This implies that the absorption of the disturbance must be minimal for propagation in the north-south direction. This is due to the fact that J'E is small when the neutral wind disturbance is nearly parallel to the magnetic field. For  $\alpha$  large (high to mid-latitudes),  $R_m = G \sin^2\alpha$  and  $R_m/R_z \sim 1$ . Thus, at high and mid-latitudes all the directions of propagation of moving disturbances are approximately equivalent with respect to magnetohydrodynamic absorption. Consequently  $R \sim G$ . So, using Table 1 and considering that the absorption can be expressed by  $\exp -R$ , we can find the distances

$$D \approx 1/G \quad (4)$$

at which the wave amplitude decreases by a factor of  $e$ . At a height  $h = 220$  km, that can represent the F-layer bottomside, we have  $D = 3000$  km and, consequently, the DBS take around 3 hours to be completely dissipated (considering the phase velocity  $V_{ph} = \omega / k_x = 250$  m/s). This space-time estimation of the DBS lifetime seems to be reasonable and agrees with the DBS shown in Figure 7. On the other hand, around the F-layer peak ( $h = 300$  km), we have  $D = 600$  km and, consequently, the DBS take around 40 minutes to be completely dissipated. The above absorption estimates indicate that the distance of propagation of DBS does not generally exceed 3000 km.

It can be expected (Table 1) that maximum absorption take place in the vicinity of the F layer maximum. From this point of view we can understand the fact that most moving disturbances covering distances of several thousands of kilometers (for example, the event on August 30-31, 1995) are recorded probably at heights below this maximum. However, our observations sometimes show DBS events propagation approximately toward the west direction, thus reinforcing the idea that the effects of the ionization on its propagation in the nighttime ionosphere is more important than the orientation of the direction of propagation relative to the  $\mathbf{B}$  field.

We close this section with the proviso that if the DBS become electrified as seems to be the case, the magnetohydrodynamic damping will decrease and in the fully polarized state  $\mathbf{E} \times \mathbf{B} = \mathbf{U}$  and ion drag ceases. Turning this argument around, Kelley and Miller (1997) noted that propagation in the Perkins' direction is just the right direction to minimize the damping.

*On the Perkins Process.* We conjecture that the Perkins instability might be involved in the formation of DBS structures. The most notable feature of the structures reported here is their tendency to be aligned from northeast to southwest and drift towards the northwest in the southern hemisphere as found in the present observations as well as in other studies quoted in this paper. Perkins, (1973), created a model to study a possible instability of the mid-latitude ionosphere [see Perkins (1973), Kelley and Miller, (1997); Hamza, (1999); Garcia et al., (2000), for Perkins instability theory]. It should be noted that the ionospheric Perkins instability, which is a possible cause of MSTIDs, is an electrostatic instability based on the coupling between ionospheric current and conductivity to develop electric field and conductivity oscillations. This instability can be seeded by neutral wind oscillation, such as gravity waves. However, this neutral wind oscillation is just to give an initial perturbation for the electrostatic instability.

Behnke (1979), using the Arecibo radar in an incoherent scatter mode, reported that localized bands in the F-region ionosphere moved from northeast to southwest across the observed region (in the northern hemisphere). This is the same direction reported for the angle-of-arrival measurements of classic mid-latitude spread-F by a number of researchers using ionosonde techniques. As discussed by Kelley and Fukao, (1991), the great preponderance of angle-of-arrival data suggests that the disturbances in the ionosphere, which cause mid-latitude spread-F, are such that in the southern hemisphere the preferred direction is from the southeast while in the northern hemisphere it is from the northeast. In addition, the occurrence rate of mid-latitude spread-F has considerable annual and also solar-cycle variations (Bowman, 1960). Also, Kelley and Fukao (1991) showed that the growth rate determined by Perkins is considerably higher during sunspot minimum conditions than during sunspot maximum for comparable altitudes of the ionospheric F-layer, and this is consistent with our observations (our events were observed during low solar activity and ascending solar activity periods). However, more observations are needed to further clarify the generation mechanism (seeding and growth phase) of the DBS as well as the damping phase discussed above.

#### **4 - Conclusions**

Measurements of the two-dimensional properties of Dark Band Structures (DBS) in the nighttime thermosphere/ionosphere are presented. The observed features of the DBS can be summarized as follows:

- 1 - The most notable feature of the structures reported here is their tendency to be aligned from northeast to southwest and to drift towards the northwest at an altitude approximately of 220-350 km.
- 2 - It should be pointed out that these thermospheric events are not related to geomagnetic disturbed conditions.
- 3 - Estimates of the spatial damping decrement for AGW's show that the increase in absorption is associated mainly with the increase in electron concentration (for example, the event on July 19, 1998). It can be expected (Table 1) that maximum absorption takes place in the vicinity of the F-layer maximum. From this point of view we can understand the fact that most moving disturbances covering distances of several thousands of kilometers (for example, the events on August 30-31, 1995) are recorded probably at heights below this maximum.
- 4 - We conjecture that the Perkins instability might be involved in the formation of DBS structures and that the Perkins direction has minimum damping. Clearly, more observations are needed to further clarify the generation mechanism and damping of the DBS.

**Acknowledgement:** We would like to thank the Ionosphere Group at INPE for kindly providing the ionospheric parameters obtained at Cachoeira Paulista, and to Professors M. Mendillo and M. J. Taylor for the use of the OI 630 nm images presented in this work. Also, the authors acknowledge the Conselho Nacional de Desenvolvimento Científico e Tecnológico (CNPq) through process 476937/2006-0.

## References

- Behnke, R. F-layer height bands in the nocturnal ionosphere over Arecibo. *Journal of Geophysical Research*, p. 974-978, 1979.
- Bowman, G.G. Further studies of spread-F at Brisbane.2. Interpretation. *Planetary and Space Science*. 2(2-3):p.150-156, 1960.
- Colerico, M., M. Mendillo, D. Nottingham, J. Baumgardner, J. Meriwether, J. Mirick, B.W. Reinisch, J.L. Scali, C.G. Fesen, and M.A. Biondi. Coordinated measurements of F-region dynamics related to the thermospheric midnight temperature maximum, *Journal of Geophysical Research*, v. 101, p. 26,783-26,793, 1996.
- Colerico, M. and M. Mendillo. The current state of investigations regarding the thermospheric midnight temperature maximum (MTM). *J. Atmos. Solar-Terr. Phys.*, 64, 1361,1369, 2002.
- Dalgarno, A. and J.C.G. Walker. The red line of atomic oxygen in the day airglow. *J. atmos. Sci.* 21, 463-474, 1964.
- Gamache, R.R., B.W. Reinisch, and W.T. Kersey. ARTIST electron density profile algorithm, *Sci. Rep.* 468, Cent. For Atmos. Res., Univ. of Mass., Lowell, 1992.
- Garcia, F.J., M.J. Taylor, M.J. Kelley. Two-dimensional spectral analysis of mesospheric airglow image data. *Applied optics*, v.36, p.7374-7385, 1997.
- Garcia, F.J., M.C. Kelley, and J.J. Makela. Airglow observations of mesoscale low-velocity traveling ionospheric disturbances at mid-latitudes. *Journal of Geophysical Research*, p. 18,407-18415, 2000.
- Dewan, E.M., Picard, R.H. On the origin of mesospheric bore. *Journal of Geophysical Research*, 106, 2921-2927, 1998.
- Gershman, B.N. and G.I. Grigor'yev. Theory of moving ionospheric disturbances. *Geomagnetism and Aeronomy*, v.5, p.2248-2255, 1965.
- Hamza, A.M. Perkins instability revisited. *Journal of Geophysical Research*, v.104, p. 22,567-22,575, 1999.
- Hines C.O., Hooke W.H. Internal atmospheric gravity waves at ionospheric heights. *Canadian Journal of Physics*, 38, 1441-1481, 1960.
- Hines, C.O., Discussion of ionization effects on the propagation of acoustic-gravity waves in the ionosphere. *Journal of Geophysical Research*, v.75, p. 2563-2567, 1970.
- Hunsucker, R.D. Atmospheric gravity waves generated in the high latitude ionosphere: A review, *Res. Geophys.*, 20, 293-315, 1982.
- Mendillo, M. and Baumgardner, J. Airglow characteristics of equatorial plasma depletions. *Journal of Geophysical Research*, 87, p. 7641-7652, 1982.
- Mendillo, M., J. Baumgardner, D. Nottingham, J. Aarons, B. Reinisch, J. Scali, M. Kelley. Investigations of thermospheric-ionospheric dynamics with OI 630 nm images from the Arecibo observatory. *Journal of Geophysical Research*, v. 102, p. 7331-7343, 1997.

Nicolls, M.J., M.C. Kelley, A. J. Coster, S.A. Gonzales, J.J. Makela. Imaging the structure of a large-scale TID using ISR and TEC data, *Geophysical Research Letters* 31 (9): Art. No LO9812, 2004.

Perkins, F. Spread F and ionospheric currents. *Journal of Geophysical Research*, v.78, p. 218-226, 1973.

Pimenta, A.A., Fagundes, P.R, Bittencourt, J.A., Sahai, Y., Gobbi, D., Medeiros, A.F., Taylor, M.J., Takahashi, I. Ionospheric plasma bubble zonal drift: a methodology using OI630 nm all-sky imaging systems. *Adv. Space Res.* Vol. 27, n 6-7, p. 1219-1224, 2001.

Kelley, M.C and S.Fukao. Turbulent upwelling of the mid-latitude ionosphere 2. Theoretical framework. *Journal of Geophysical Research*, v.96, p. 3747-3753, 1991.

Kelley, M.C., C.A. Miller. Electrodynamics of mid-latitude spread-F, 3, Electrohydrodynamic waves? A new look at the role of electric fields in thermospheric wave dynamics. *Journal of Geophysical Research*, v.102, p. 11,539-11,547, 1997.

Kelley, M.C., J.J. Makela, E. W.E. Swartz, S.C. Collins. Caribbean Ionosphere Campaign, Year One: Airglow and plasma observations during two intense mid-latitude spread-F events, *Geophysical Research Letters*, v.27, p. 2825-2828, 2000.

Kelley, M.C., J.J. Makela, A. Saito. The mid-latitude F-region at the mesoscale: some progress at last. *Journal of Atm. And Solar-Terrestrial Physics*. P. 1525-1520, 2002.

Saito, A., T. Iyemori, M. Takeda and M. Yamamoto. Conjugate occurrence of the electric field fluctuations in the nighttime mid-latitude ionosphere, *Journal of Geophysical Research*, v.100, p. 21,439-21,451, 1995.

Shiokawa, K., Y. Otsuka, T. Tsugawa, T. O gawa, A. Saito, K. Ohshima, M. Kubota, T. Maruyama, T. Nakamura, M. Yamamoto, P. Wilkinson. Geomagnetic conjugate observation of nighttime medium-scale and large-scale traveling ionospheric disturbances: FRONT3 campaign. *Journal of Geophysical Research*, v.110, A05303, doi:10.1029/2004JA010845, 2005.

Sobral, J.H.A., G.L. Borba, M.A. Abdu, I.S. Batista, H. Sawant, c.j. Zamlutti, H. Takahashi and Y. Nakamura. Post-sunset wintertime 630.0 nm airglow perturbations associated with gravity waves at low latitudes in the South American sector. *Journal of Atmospheric and Solar-Terrestrial Physics*, v.59, p.1611-1623, 1997.

Taylor, M.J., D.N. Turnbull, R.P. Lowe. Spectrometric and imaging measurements of a spectacular gravity wave event observed during the ALOHA-93 campaign. *Geophysical Research Letters*, v.22, p.2849-2852, 1995.

Titheridge, J.E. Theory of moving ionospheric disturbances, *Journal of Geophysical Research*, p.656-660, 1973.

Titheridge, J.E., The relative accuracy of ionogram analysis techniques, *J. Atmos. Terr. Phys.*, 10, p.589-599, 1975.

Fig. 1. OI 630.0 nm emission all-sky image obtained at Cachoeira Paulista, Brazil, on August 31, 1995, at 00:20 LT, with its respective field of view (considering an emission height around 275 km).

Fig. 2. (A) 512x512 pixel resolution all-sky image showing DBS in the OI 630.0 nm airglow emission. (B) example of unwarping all-sky image of Figure 2A using the method described by Garcia et al. (1997). In this figure, an area of the processed image, corresponding to 360,000 km<sup>2</sup> (600 km x 600 km) at the airglow layer, is mapped assuming an emission altitude of 275 km. (C) Computed squared magnitude of 2-D FFT of the image inside the square border in Fig. 2B.

Fig. 3. DBS observed through the airglow OI 630 nm emission on the night July 19, 1998, from 26:00 LT to 27:20 LT at Cachoeira Paulista. Note that the DBS was resolved as a series of wave crests ( $\lambda_n = 100$  km) at 26:40 LT and then, later, was totally dissipated. The arrows indicate the wave structures in the all-sky images.

Fig. 4. (A) F-layer peak height ( $h_m F_2$ ) and base height ( $h'F$ ) on July 18-19, 1998. (B) Digisonde observations of  $f_o F_2$  (electron density).

Fig. 5. DBS observed by the airglow OI 630 nm emission on the night July 13, 1999, from 21:47 LT to 23:55 LT at Cachoeira Paulista using all-sky imager.

Fig. 6. (A) F-layer peak height ( $h_m F_2$ ) and base height ( $h'F$ ) time series on July 13-14, 1999, used for the wavelet analysis. (B) Digisonde observations of  $f_o F_2$  (electron density). (C) The local wavelet power spectrum of  $h_m F_2$  using the Morlet wavelet.

Fig. 7. All-sky images in the OI 630 nm emission obtained on August 30-31, 1995, from 22:40 to 25:00 LT. In this example, the DBS entered from the southeast and moved across the field of view towards northwest, with an average speed of about 250 m/s.

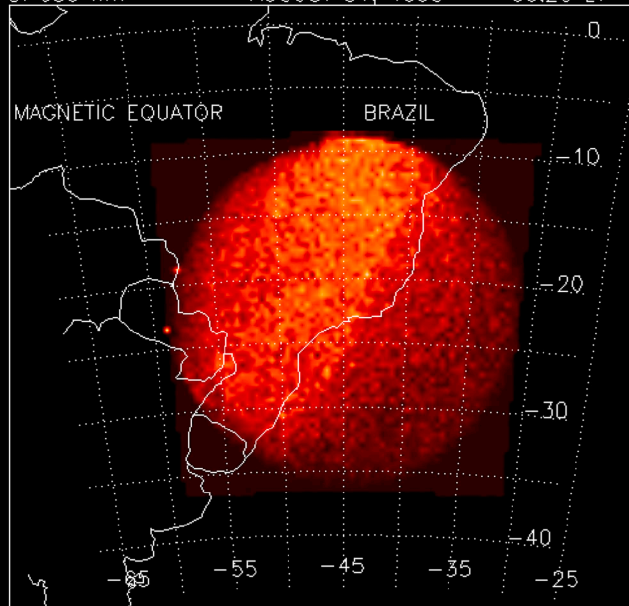
Table1 – G values in cm<sup>-1</sup> for various heights, corresponding to the F-layer of the ionosphere.

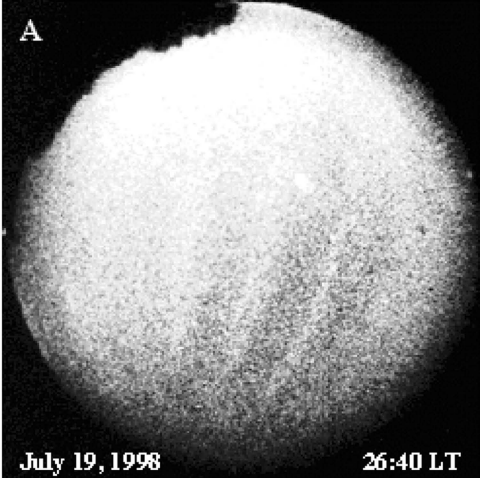
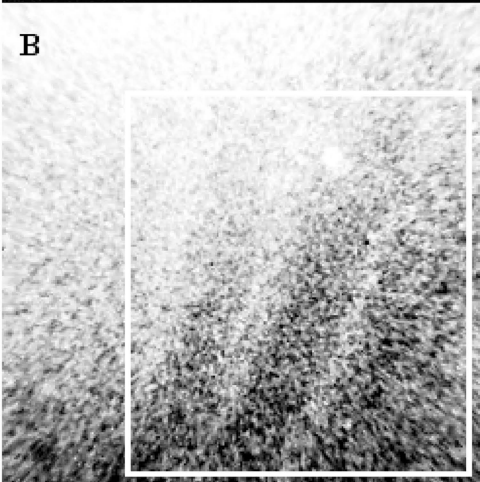
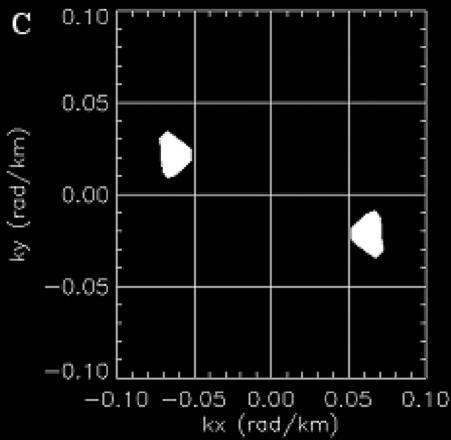
Altitude (km)	$V_{ph}$ (m/s)	G (in cm <sup>-1</sup> )
220	250	$3.3 \times 10^{-9}$
250	250	$7.0 \times 10^{-9}$
300	250	$1.6 \times 10^{-8}$

OI 630 nm

AUGUST 31, 1995

00:20 LT

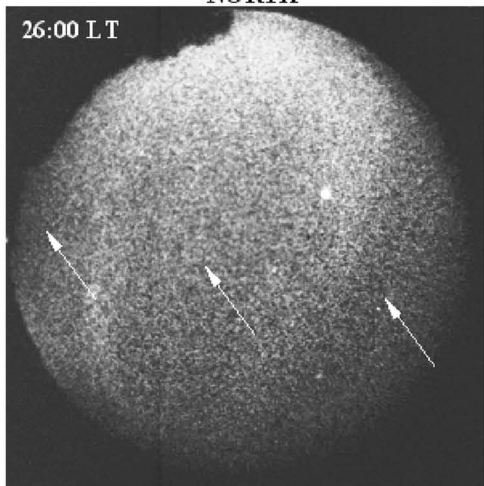


**A****July 19, 1998****26:40 LT****B****C**

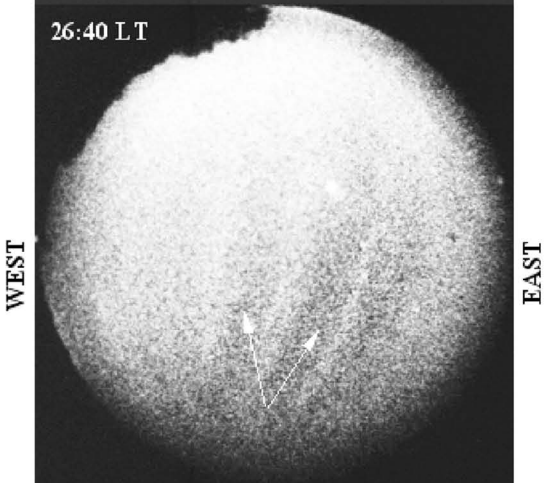
Cachoeira Paulista, July 19, 1998

NORTH

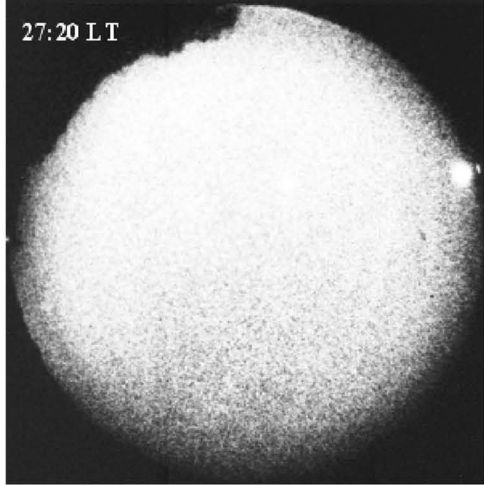
26:00 LT



26:40 LT

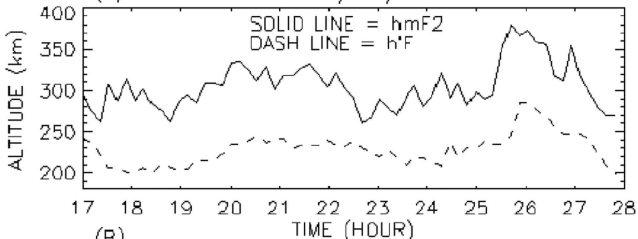


27:20 LT

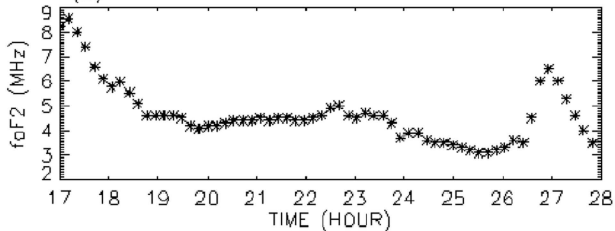


SOUTH

(A) 18-19/07/1998



(B)



Cachoeira Paulista, July 13, 1999

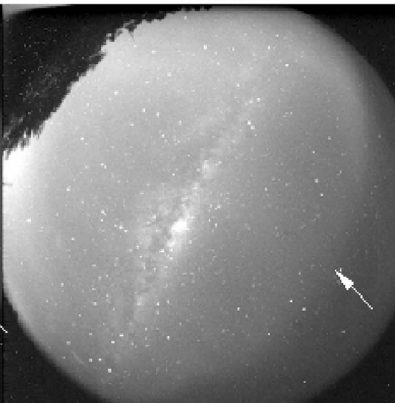
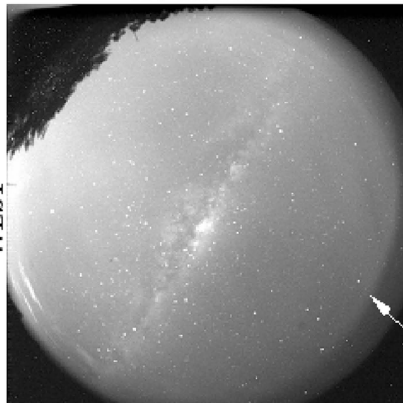
630 21:47:15 LT

**SOUTH**

630 23:20:02 LT

630 23:55:43 LT

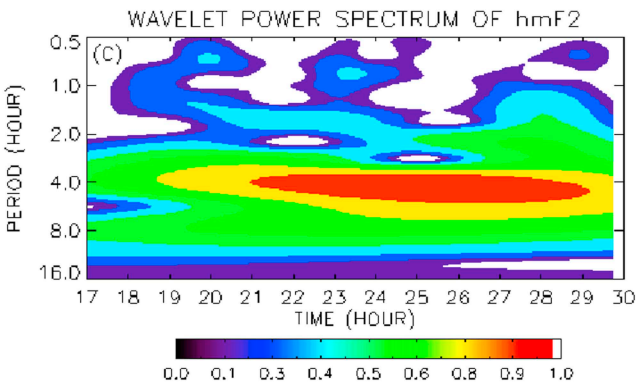
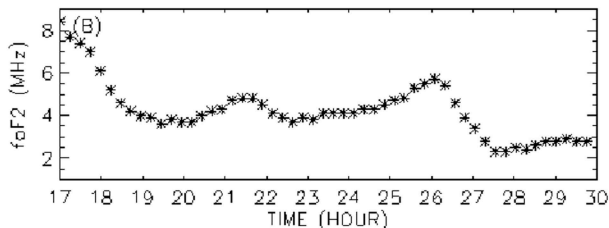
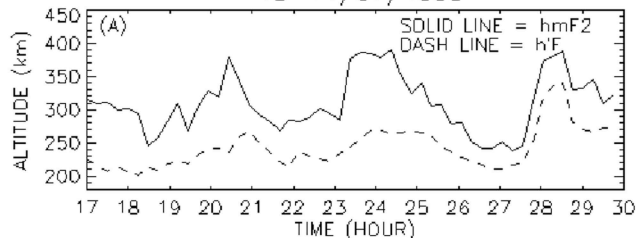
**WEST**



**EAST**

**NORTH**

13-14/07/1999



Cachoeira Paulista, August 30-31, 1995

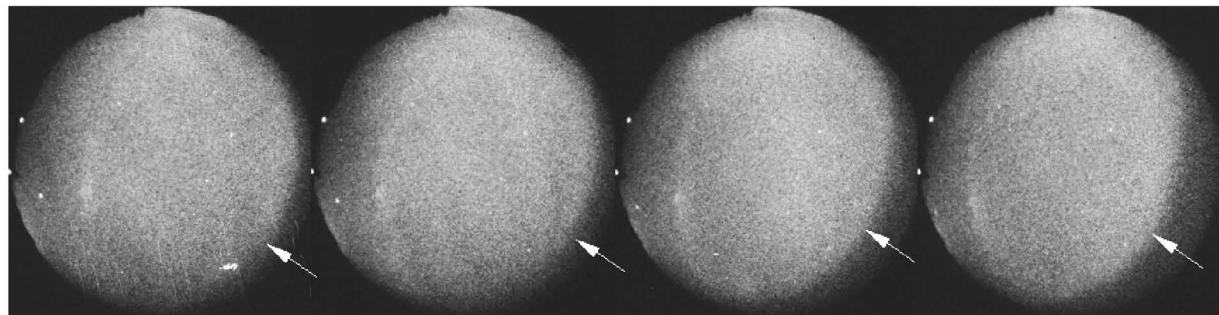
22:40 LT

23:00 LT

NORTH

23:20 LT

23:40 LT

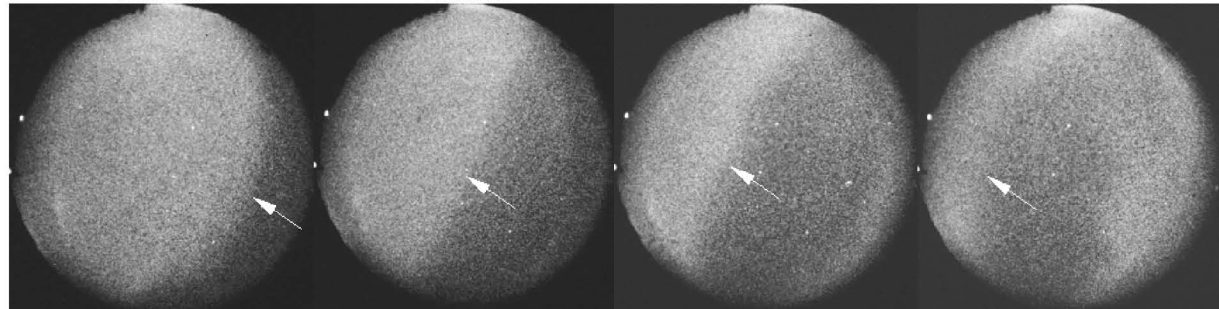


24:00 LT

24:20 LT

24:40 LT

25:00 LT



SOUTH